TWENTY FIFTH EUROPEAN ROTORCRAFT FORUM

Paper no. C13

ACTIVE SUPPRESSION OF STALL ON HELICOPTER ROTORS

BY

KHANH NGUYEN
ARMY/NASA ROTORCRAFT DIVISION
NASA AMES RESEARCH CENTER, MOFFETT FIELD, CA

SEPTEMBER 14-16, 1999
ROME
ITALY

ASSOCIAZIONE INDUSTRIE PER L'AEROSPAZIO, I SYSTEMI E LA DIFESA
ASSOCIAZIONE ITALIANA DI AERONAUTICA ED ASTRONAUTICA

Active Suppression of Stall on Helicopter Rotors

Khanh Nguyen
Army/NASA Rotorcraft Division
NASA Ames Research Center, Moffett Field, CA

Abstract

This paper describes the numerical analysis of a stall suppression system for helicopter rotors. The analysis employs a finite element method and includes advanced dynamic stall and vortex wake models. The stall suppression system is based on a transfer function matrix approach and uses blade root actuation to suppress stall directly. The rotor model used in this investigation is the UH-60A rotor. At a severe stalled condition, the analysis predicts three distinct stall events spreading over the retreating side of the rotor disk. Open loop results show that 2P input can reduce stall only moderately, while the other input harmonics are less effective. The responses of the stall index, a measure of stall, to individual input harmonics are highly nonlinear. Such nonlinear stall behavior makes the closed-loop controller ineffective in suppressing stall and the combined effects of individual harmonics non-additive. Also, stall reduction does not guarantee gains in rotor performance.

1. Introduction

Active control has the potential to directly suppress rotor blade stall and thus can expand the helicopter flight envelope. Unlike fixed-wing aircraft, stall does not limit the low speed operation of helicopters. Stall on rotor blades limits the rotor structural envelope, in particular, the helicopter maximum speed and the rotor loading capabilities. At the stall boundary, the large blade pitching moment induced by stall can cause stall flutter and excessive loading, leading to fatigue of structural components. In addition, stall increases the rotor shaft torque, causes excessive vibration, and adversely affects the aircraft handling qualities. Successful control of stall can enhance the utility of rotorcraft.

Classical treatments of rotor stall indicate that stall typically occurs near the retreating blade tip. In forward flight, a blade encounters a time-varying dynamic pressure due to the combined effects of blade rotation and vehicle forward speed. Thus, the dynamic pressure is greater on the advancing side than the retreating side. To balance the roll moment on the rotor, the basic trim control provides low angle of attack on the advancing side and high angle of attack on the retreating side. As the rotor loading or the forward speed increases, stall is initiated due to the large angle of attack requirement on the retreating side.

Operating in an unsteady environment, the blade encounters the most severe type of stall known as dynamic stall. In forward flight, the blade experiences time-varying dynamic pressure and angle of attack arising from blade pitch inputs, elastic responses, and non-uniform rotor inflow. If supercritical flow develops under dynamic conditions, then dynamic stall is initiated by leading edge or shock-induced separation. Even with limited understanding about the development of supercritical flow in the rotor environment, flow visualization results of oscillating airfoil tests at low Mach number suggest that supercritical flow is associated with the bursting of the separation bubble as it encounters the large adverse pressure gradient near the blade leading edge [1]. Dynamic stall is characterized by the shedding of strong vortices from the leading edge region. The leading edge vortex produces a large pressure wave moving aft on the airfoil upper surface and creating abrupt changes in the flow field. The pressure wave also contributes to large lift and moment overshoots in excess of static values and prolongs flow separation, both causing significant nonlinear hysteresis in the airfoil behavior.

The other type of stall typically observed in two-dimensional wind tunnel tests involves trailing edge separation. The phenomenon of trailing edge separation is associated with either static or dynamic conditions. Separation starts from the airfoil trailing edge, and with increasing angle of attack, the separation point progresses towards the leading edge region. Trailing edge separation contributes to nonlinear behavior, such as hysteresis, in lift, drag and pitching moment due to the loss in circulation. In contrast to dynamic stall that is characterized by abrupt changes in airfoil behavior, trailing edge stall progresses at a moderate rate.

A recent investigation of blade pressure data from the UH-60A Airloads Program [2] has helped improve understanding about rotor stall behavior. Test results reveal that stall is not confined solely to the retreating side but rather spreads to the first quadrant of the rotor disk. Since stall is strongly coupled with the blade dynamics, especially the torsion mode, this coupling manifests in a stall cycle that begins in the fourth quadrant of the rotor disk and continues up to the first quadrant in two cycles (three stall peaks). The stall cycle has a frequency

closely matched with the blade torsion frequency. Flight test data also indicate that rotor stall exhibits behavior similar to that observed in airfoil oscillating tests where the shedding of the strong leading edge vortex dominates the flow pattern.

Passive control of blade stall typically employs the tailoring of blade twist and planform for efficient blade load distribution. Modern rotors often employ blade construction with multi-airfoil sections -- thick, high-lift sections inboard and thin, transonic sections for the tip region. These designs aim to provide efficient rotor disk loading and low drag and thus, are employed primarily for performance benefits; however, they also provide stall alleviation. The design of the BERP rotor [3] is one notable example of passive methods. The BERP blade has multiple airfoil sections and a prominent tip shape designed to operate efficiently in the transonic regime (low angle of attack advancing blade tip) and to generate high lift in subsonic flow condition (retreating blade tip).

In an effort to expand the helicopter flight envelope, this analytical study explores the use of high frequency blade pitch actuation to alleviate blade stall. The availability of high-frequency blade-mounted actuators has made active stall suppression realizable. Earlier investigations of active rotor control have focussed on swashplate actuation [4]. This scheme places a limit on the number of harmonics available for excitation at $N-1$, N, and $N+1$ per rev, where N is the number of blades per rotor. With the blade-mounted actuators, the excitation frequency is not limited by the swashplate constraint but by the bandwidth of the actuators. ZF Luftfahrttechnik GmbH of Germany built and flight-tested an individual-blade-control type actuator with excitation frequencies varying from two to twelve per rev on an MBB BO-105 helicopter [5]. More recently, the same company is building larger actuators to be retrofitted into a full-scale UH-60A rotor for wind tunnel testing at NASA Ames.

2. Previous Stall Suppression Works

In the fifties and early sixties, Stewart [6], Payne [7], and Arcidiacono [8], conducted separate analyses to investigate the potential of using higher harmonic control to delay the onset of retreating blade stall. These investigators discovered that higher harmonic control could be used in combination with the basic trim control to redistribute lift on the rotor. Such lift redistribution could be adjusted to relieve retreating blade stall while maintaining the rotor trim states. The resulting effect would be to raise the speed limitation of helicopters.

In 1961, Bell Helicopter Company conducted a flight test on an UH-1A helicopter equipped with a rotor head mechanism capable of generating two-per-rev blade pitch [9]. The test explored the potential of 2P blade pitch to improve rotor performance and cabin vibration. Test results showed no reduction in the rotor shaft torque with any combinations of amplitude and phase of the 2P input. A post-test analysis revealed that the drag reduction on the retreating side due to 2P control was offset by an increase in profile drag in the fore and aft portions of the rotor disk. Even though stall alleviation was not attempted in the test program, such conclusions confirmed the previous analytical predictions that 2P control could be used to redistribute the rotor loading.

In the early eighties, Kretz [10] wind tunnel tested a "stall barrier feedback" system on a six-foot diameter two-bladed rotor for stall suppression. The system relied on three pressure sensors mounted at 85 percent blade radial station to monitor stall. The pressure sensors provided feedback signals that activated the high frequency actuators to avoid stall. The feedback pressure signals were based on the threshold values adapted from airfoil test data. Test results yielded no concrete conclusions to substantiate the benefits of this stall suppression system.

3. Scope of Current Investigation

The objective of the current study is to analytically evaluate the effectiveness of an automatic stall suppression system for helicopters using higher harmonic blade root input. The effects of stall suppression on rotor performance are also investigated. Stall suppression is formulated as an optimization problem in which the stall behavior of a rotor is quantified and subsequently minimized using higher harmonic control (HHC). Thus, the system suppresses stall directly.

In this paper, the term higher harmonic control refers to blade pitch input with harmonic content greater than one per-rev. Since the focus of the paper is on the aerodynamic performance aspects of stall suppression, the effects of HHC on blade loads, control system loads, and vibratory hub loads, which can be significant, are not discussed.

The analysis used in this study will be described, followed by a description of the HHC system for stall suppression. The analysis is then used to model a stalled condition for the UH-60A rotor. An evaluation of the open and closed-loop stall suppression system is provided. Finally, specific findings from this study are presented.

4. Aeroelastic Analysis

The NASA Ames-version of the University of Maryland Advanced Rotorcraft Code (UMARC) [11] is adopted to investigate the potential of active control to suppress rotor stall. UMARC/A is a finite element code that includes advanced unsteady aerodynamics and vortex-wake modeling. The structural and aerodynamic modeling of UMARC/A makes

the code a suitable analysis for studying active control effects on rotor behavior.

The rotor blade is modeled as an elastic, isotropic Bernoulli-Euler beam undergoing small strain and moderate deflections. The blade degrees of freedom are flap bending, lead-lag bending, elastic twist, and axial deflections. The finite-element-method based on Hamilton's principle allows a discretization of the blade model into a number of beam elements, each with fifteen degrees of freedom.

The blade airloads are calculated using a nonlinear unsteady aerodynamic model proposed by Leishman and Beddoes [12]. This model consists of an attached compressible flow formulation along with a representation of the nonlinear effects due to trailing edge separation and dynamic stall. In the attached flow formulation, the normal force (or lift) and pitching moment includes both circulatory and impulsive (noncirculatory) components. Physically, the circulatory components model the shed wake effects, while the impulsive components originate from the pressure wave generated by the airfoil motion. For dynamic stall modeling, an artificial normal force c_N' is computed based on the attached flow lift and the dynamics of the pressure distribution, represented by a time-lag model. This quantity incorporates the effects of stall delay and is used as a criterion of stall onset.

The trailing edge separation model is based on Kirchhoff's formulation, which relates the separation location f to the airfoil force and moment behavior. The variation of the separation location with angle of attack is constructed from static airfoil data, then the results are curve-fitted. The value of the separation location is a measure of the degree of nonlinearity in the lift behavior. Information about the flow separation point also allows the reconstruction of the airfoil static behavior, a precursor to the modeling of the airfoil dynamic characteristics.

For dynamic stall, stall onset is based on the criterion that leading edge separation initiates only when the artificial normal force c_N' attains a critical value, c_{N1}, corresponding to a critical leading edge pressure. In this model, c_{N1} is the maximum lift coefficient from the airfoil tables and is a function of the Mach number. Once initiated, the excess lift due to dynamic stall is governed by the dynamics of the vortex lift, defined as the difference in lift between the attached (linear) and separated flow (nonlinear) regimes. The vortex motion over the airfoil upper surface induces a large change in the pitching moment. The vortex induced pitching moment is computed based on the vortex lift and the position of the center of pressure.

A prescribed wake model is used for the inflow calculation. The coupled blade response and trim control settings are solved for simulated wind tunnel conditions. For trim, the rotor shaft orientation is prescribed, and the blade collective and cyclic pitch inputs are automatically adjusted to desired values of thrust and hub moments or blade flapping schedules. A modal reduction technique is employed in the blade response solution to reduce the computational requirement. The modal equations are solved iteratively using a robust finite-element-in-time method in which the periodic boundary conditions are inherent in the formulation. The converged solution satisfies the governing equations for both rotor trim and blade response, which include higher harmonic control effects.

5. Higher Harmonic Control System

The controller algorithm, based on a transfer function matrix approach, is implemented in UMARC/A. Depending on the control objectives considered (to suppress stall or to reduce rotor shaft torque) each element of the transfer matrix represents the sensitivity of the controlled parameter (z) to each harmonic of the blade root actuation (u). In this investigation, the transfer matrix is computed using a finite-difference-method in which each harmonic of the control input (sine and cosine components) is perturbed individually. The control law is formulated as an optimization problem:

$$\min\ (qz_i^2 + u_i^T R u_i) \qquad (1)$$

subjected to

$$z_i = z_{i-1} + (1-r)T_i(u_i - u_{i-1}) \qquad (2)$$

In Eq. 1, the parameters q (a scalar) and R (a diagonal matrix) assign relative weightings to the controlled parameter z_i and each component of the input vector, respectively. Since the controller is based on a harmonic method, the controller cycle i is once-per-rotor revolution.

For stall suppression, z_i is the stall index computed at each controller cycle by:

$$z_i = \sum_{m}^{42} \sum_{n}^{120} F(r_m, \psi_n) \qquad (3)$$

where the double summation is over the 5040 computation points over the rotor disk (42 points in the radial direction X 120 azimuth steps), and the lift excess F is:

$$F(r,\psi) = \begin{cases} (c_N' - c_{N1})M^2 & \text{if } c_N' \geq c_{N1} \\ 0 & \text{otherwise} \end{cases} \qquad (4)$$

Note that F is defined over the entire rotor disk, with r being the blade radial station, ψ the azimuth angle, and M the local Mach number. With this definition, the stall index is a measure of the

severity of stall on the rotor disk in term of the excess lift over the stall area. The excess lift is the amount of artificial lift c_N' over the airfoil maximum lift c_{N1}, adapted from the dynamic stall model described earlier.

In Eq. 2, the control rate factor r, with value between 0 and 1, limits the control update rate, and i denotes the controller cycle. The transfer matrix updating is an option in which T_i is updated at each controller cycle, based on a secant method [13]. The T matrix updating, when used in combination with the control rate limit, helps improve the convergence of the controller when nonlinear effects dominate. This approach was successfully applied to another control problem – vibration suppression of rotors under stalled conditions – with significant nonlinearity in the model [4].

The vector u_i represents the control input that includes harmonics from 2 to 6 per rev:

$$u_i = [\theta_{2c} \quad \theta_{2s} \quad \ldots \quad \theta_{6c} \quad \theta_{6s}]^T \qquad (5)$$

In terms of the elements of u_i, the higher harmonic schedule for the *jth* blade is:

$$\theta^j_{HHC}(\psi) = \sum_{k=2}^{6} A_k \cos(k\psi^j - \phi_k) \qquad (6)$$

Besides stall suppression, a second controller is also investigated. This controller aims to improve the rotor performance using higher harmonic blade root pitch. For this system, the controlled parameter (Eq. 3) is simply the rotor shaft torque. Except for the change in the definition of z, this controller retains the same structure as that of the stall suppression controller. Note that this controller does not restrict the input harmonic to 2P as in other investigations (such as [14] or [15]) but includes a wide range of input harmonics (2P to 6P).

6. Rotor Model

This study uses the UH-60A as the rotor model. The rotor is fully-articulated with 20 deg swept tip blades. The blade is modeled with eight elastic beams along with a coincident flap-lag hinge for root boundary conditions. The pitch-link is modeled with a restraining spring. The blade sweep is not modeled explicitly, but the sweep effects are included using chordwise offsets of center of gravity and aerodynamic center. Table 1 lists the generic rotor parameters and the computed blade frequencies. The airfoil tables of the SC-1095 and the SC-1095R8 are adapted from those reported in Ref. 15.

In order to simplify the analysis, a wind tunnel trim simulation is used. The prescribed variables are the rotor shaft tilt, cyclic flappings, and rotor thrust (C_T/σ). The baseline flight condition corresponds to a C_T/σ of 0.13, advance ratio of 0.236, and 3 deg forward shaft tilt. The computed airloads are shown in Fig. 1. The lift distribution shown in Fig. 1(a) does not reveal any significant stall events. However, the drag distribution (Fig. 1(b)) suggests more than one stall event inboard of the blade midspan on the retreating side of the rotor disk. The lift excess $F(r,\psi)$, defined in Eq. 4 as a measure of stall, is shown in Fig. 1(c). This figure clearly shows that the inboard drag rises are associated with the three stall events starting near 180 deg azimuth and continuing into the first quadrant. With regards to the flight test data of Ref. 2 which shows that the three stall events occur near the blade tip, these computed results suggest that the analysis is probably deficient in the inflow modeling.

7. Open Loop Study

An open-loop study provides the sensitivity of the stall index to the amplitude and phase variation of single harmonic inputs. For each harmonic, the input phase is varied at constant amplitude, and then the amplitude at the optimum phase is varied. These results aim to provide insight into the input-output behavior of the system and help define the type of controller (linear versus nonlinear) to use. The effectiveness of the closed-loop system is also estimated based on open-loop data. Representative results are presented in this paper.

Figure 2 shows the variation of stall index to the 2P phase sweep in increment of 30 deg at 1 deg amplitude for the same flight condition (μ = 0.236, C_T/σ = 0.13) mentioned above. From Eq. 6, 210 deg phase (for minimum stall) indicates that the blade pitch is minimum at 15 and 195 deg azimuth. Since Fig. 1(c) indicates that the peak stall region occurs between 180 and 240 deg azimuth, this result suggests that stall is reduced by lowering the blade pitch at the peak stall region.

The effects of 2P amplitude variation in increment of 0.5 deg at 210 deg phase on the stall index are shown in Fig. 3. This result indicates that the stall index varies nonlinearly with the 2P amplitude. Increasing the 2P amplitude above 1 deg generates more stall. The 1 deg amplitude appears to be an optimum value for this phase angle.

For the 2P phase sweep at the same operating condition, the shaft torque variation exhibits a different trend than that of the stall index. Such results, shown in Fig. 4, indicate that the shaft torque is reduced at all phase angles of 2P input at 1 deg amplitude. While minimum stall occurs at 210 phase angle (Fig. 2), the minimum torque is at 60 deg. In fact, in the phase region where stall is minimum, the rotor shaft torque only achieves a moderate reduction compared to the minimum value at 60 deg phase.

Since the three stall events are spread over the retreating side of the rotor disk, the open loop re-

sults with the other harmonics (3P–6P) show rather complicated responses with HHC input. For example, the 3P results (Fig. 5) show two local minima for stall at 120 and at 270 deg phases. The first minimum phase input reduces the first stall event and increases the second event shown in Fig. 6(a), and vice versa for the second minimum phase input (Fig. 6(b)). Neither input phase causes significant stall reduction. The maximum stall case is shown in Fig. 6(c), in which the 30 deg phase input increases the first stall event significantly while reducing the second event by only a small amount. The 4P input can increase stall significantly while reducing stall only moderately with variation in phase at 0.7 deg of 4P amplitude. The 5P input is less effective than the 4P input, while the 6P input, like the 3P component, shows little potential to reduce stall. Results of the open loop study with individual blade pitch harmonics from 2P–6P suggest that 2P is the most effective type of input for stall reduction for this flight condition.

8. Closed Loop Study

For the closed loop study, the analysis employs trial open loop input to generate the transfer function and then operates automatically to minimize the stall index (Eq. (3)). The HHC amplitude (the RMS value of all harmonics) is constrained to be less than 3 deg. This study yields no satisfactory stall reduction. Different combinations of the number of input harmonics yield results that, at best, match the open loop 2P results shown above. A typical closed loop result using a controller with 2P and 4P input is shown in Fig. 7. This figure shows the stall index variation with the controller cycle. The controller reduces stall only by a small amount at the first cycle and then converges to a steady state value larger than the uncontrolled value. Using transfer matrix updating only causes a periodic shooting of the stall index above the steady-state value. Since 2P and 4P are the two best individual inputs for stall reduction, these results suggest that the combined effects of the different input are not additive for stall reduction. In particular, the combination of 2P and 4P input does not reduce the stall but rather generates more stall. The nonlinear behavior associated with active stall control for this rotor system would require a more robust, nonlinear controller.

The same controller performs quite satisfactorily when used to reduce the rotor shaft torque with 2P input. Again, the HHC amplitude is constrained to be less than 3 deg. The result is shown in Fig. 8. The controller using 2P input converges to a steady 7.2 percent reduction in shaft torque. The transfer matrix update algorithm causes a small deviation at the 5th controller cycle.

9. Concluding Remarks

Analytical study of stall suppression for a UH-60A rotor is conducted at a moderate forward speed ($\mu = 0.236$) and high thrust ($C_T/\sigma = 0.13$) condition. The UMARC/A analysis predicts three distinct stall events spreading over the retreating side of the rotor disk for this flight condition. The results of this investigation show that stall on the UH-60A rotor can be reduced only moderately with higher harmonic control at this stalled condition. Open loop results show that 2P input can reduce stall moderately, while the other input harmonics are less effective. The responses of the stall index, a measure of stall, to individual input harmonic are highly nonlinear. Such nonlinear behavior makes the closed-loop controller ineffective in suppressing stall and the combined effects of individual harmonics non-additive.

Furthermore, since stall is only one of the phenomena affecting rotor performance, stall reduction does not guarantee a gain in rotor performance (i.e., reduction in shaft torque at constant operating conditions). The blade pitch schedule that improves rotor performance would be different from the one that reduces stall.

For future plans, this study will include better inflow models to improve the stall prediction capabilities of the UMARC/A analysis. Also, the study will focus on the stall reduction potential of HHC at higher forward speeds. High speed flight conditions may exhibit different stall patterns that can be suppressed more effectively with active control than the flight condition considered in this paper.

References

1. McCroskey, W. J., Carr, L. W., and McAlister, K. W., "Dynamic Stall Experiments on Oscillating Airfoils," *AIAA Journal*, Vol. 14, No. 1, 1976, pp. 57-63.
2. Bousman, W. G., "A Qualitative Examination of Dynamics Stall from Flight Test Data," *Journal of the American Helicopter Society*, Vol. 43, No. 4, 1998, pp. 279-295.
3. Perry, F. J., "Aerodynamics of the World Speed Record," Proceedings of the American Helicopter Society 43rd Annual Forum, St. Louis MO, May 1987.
4. Nguyen, K. and Chopra, I., "Application of Higher Harmonic Control to Rotors Operating at High Speed and Thrust," Journal of the American Helicopter Society, Vol. 35, No. 3, 1990, 336-342.
5. Richter, P. and Eisbrecher, H. D., "Design and First Flight Tests of Individual Blade Control Actuators," Proceedings of the Sixteenth European Rotorcraft Forum, Glasgow, UK, Sep 1990.

6. Stewart, W., "Second Harmonic Control on the Helicopter Rotor," Aeronautical Research Council, RM-2997, London, Aug 1952.
7. Payne, P. R., "Higher Harmonic Rotor Control," *Aircraft Engineering*, Vol. 30, No. 354, 1958, pp. 222-226.
8. Arcidiacono, P. J., "Theoretical Performance of Helicopters Having Second and Higher Harmonic Feathering Control," *Journal of the American Helicopter Society*, Vol. 6, No. 2, 1961, pp. 8-19.
9. Drees, J. M. and Wernicke, R. K., "An Experimental Investigation of a Second Harmonic Feathering Device on the UH-1A Helicopter," United States Army Transportation Research Command, TR-62-109, Fort Eustis, VA, June 1963.
10. Kretz, M., "Active Expansion of Helicopter Flight Envelope," Proceedings of the Fifteenth European Rotorcraft Forum, Amsterdam, The Netherlands, Sep 1989, Paper No. 53.
11. Gunjit, S. B., Chopra, I., and Nguyen, K., "Development of UMARC (University of Maryland Advanced Rotorcraft Code)," Proceedings of the American Helicopter Society 46th Annual Forum, Washington, D.C., May 1990.
12. Leishman, J. G., and Beddoes, T. S., "A Semi-Empirical Model for Dynamic Stall," *Journal of the American Helicopter Society*, Vol. 34, No. 3, 1989, pp. 3-17.
13. Dennis, J. E., Jr. and Schnabel, R. B., *Numerical Method for Unconstrained Optimization and Nonlinear Equations*, Prentice Hall, New Jersey, 1983, pp. 168-193.
14. Jacklin, S., Nguyen, K., Blaas, A., Richter, P., "Full Scale Wind Tunnel Test of a Helicopter Individual Blade Control System," Proceedings of the American Helicopter Society 50th Annual Forum, Washington, D.C., May 1994.
15. Nguyen, K. and Chopra, I., "Effects of Higher Harmonic Control on Rotor Performance and Control Loads," *Journal of Aircraft*, Vol. 29, No. 3, 1992, pp. 336-342.
16. Shanley, J. P., "Validation of UH-60A CAMRAD/JA Input Model," SER-701716, Nov 1991.

Table 1 Blade and rotor properties

Number of blades	4
Blade radius, R	26.833 ft
Blade airfoils	
0.48R–0.84R	SC-1095R8
other stations	SC-1095
Flapping hinge offset	0.0468 R
Rotor solidity	
Thrust weighted, σ	0.08317
Blade pretwist	Nonlinear
equivalent linear rate	-15.67 deg
Computed blade frequencies, per rev	
(@ 258 rpm and 10 deg $\theta_{.75}$)	
Rigid lag	0.283
Rigid flap	1.039
First elastic flap	2.779
First torsion	4.011
First elastic lag	4.538
Second elastic flap	5.021

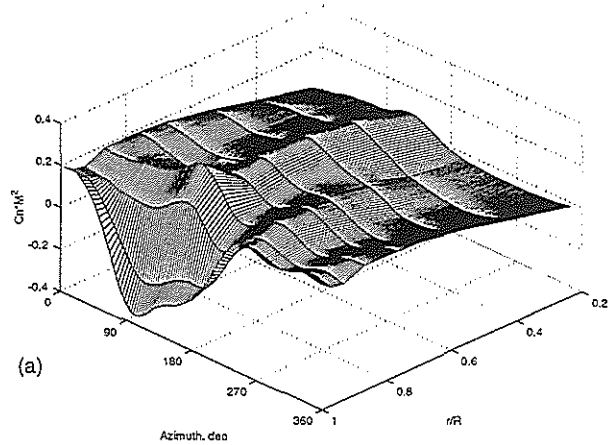

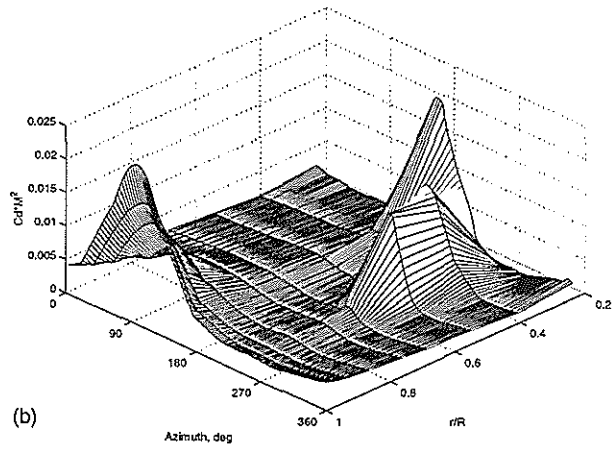

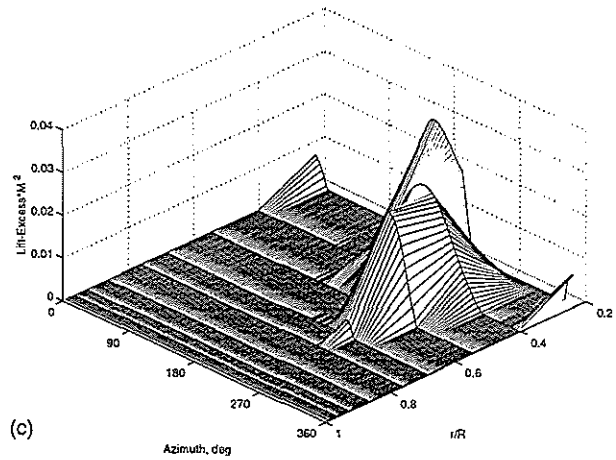

Fig. 1. Blade airloads over rotor disk: (a) normal force (or lift), b) drag, c) lift excess F(r,ψ) (μ = 0.236, $C_T/\sigma = 0.13$).

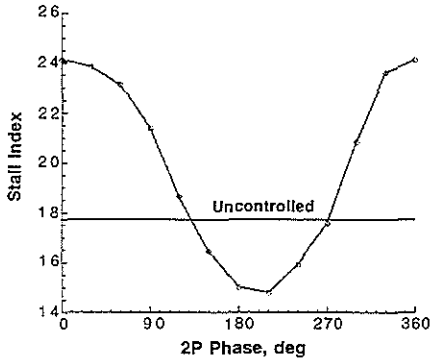

Fig. 2. Variation of stall index with 2P phase, 1 deg amplitude (μ = 0.236, $C_T/\sigma = 0.13$).

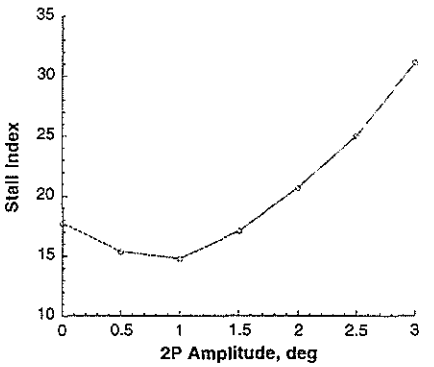

Fig. 3. Variation of stall index with 2P amplitude, 210 deg phase angle (μ = 0.236, $C_T/\sigma = 0.13$).

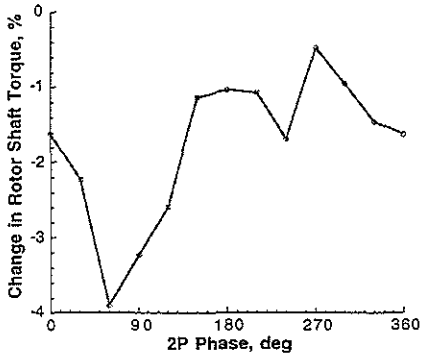

Fig. 4. Reduction in rotor shaft torque with 2P phase angle, 1 deg amplitude (μ = 0.236, $C_T/\sigma = 0.13$).

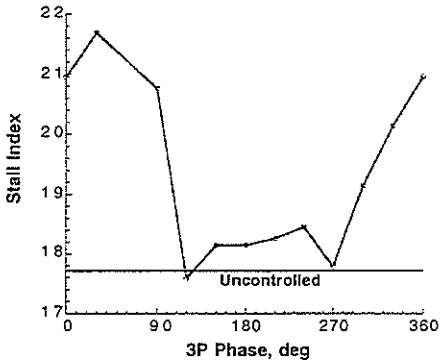

Fig. 5 Variation of stall index with 3P phase angle, 0.7 deg amplitude ($\mu = 0.236$, $C_T/\sigma = 0.13$).

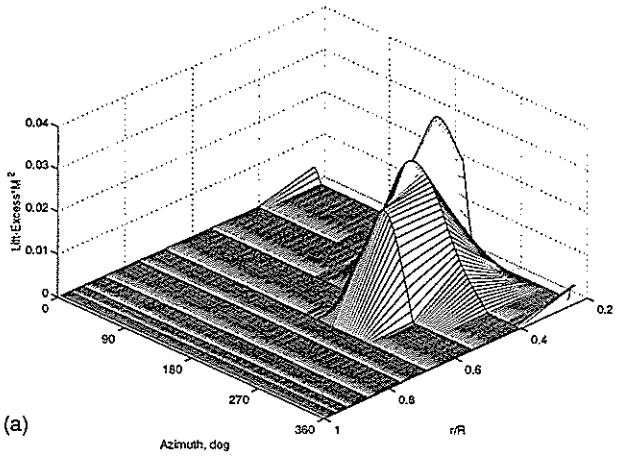

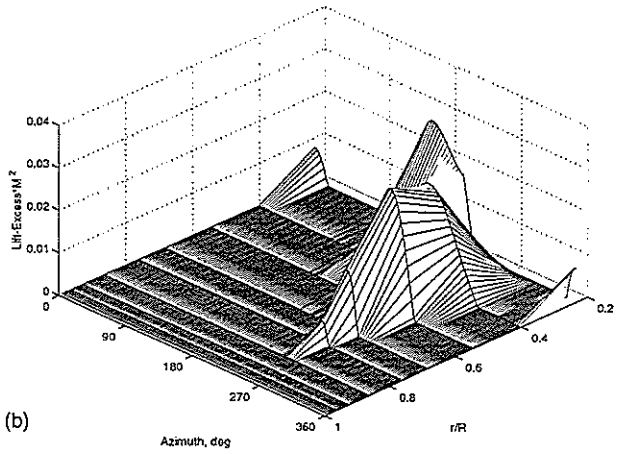

Fig. 6. Lift excess over rotor disk: (a) 120 deg 3P phase, (b) 270 deg 3P phase, (c) 30 deg 3P phase ($\mu = 0.236$, $C_T/\sigma = 0.13$).

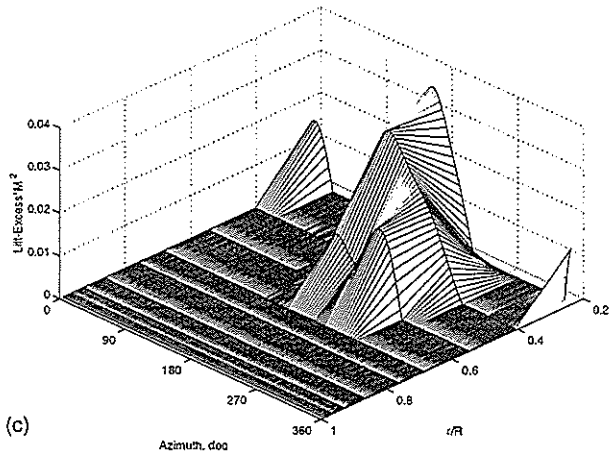

Fig. 6. Concluded.

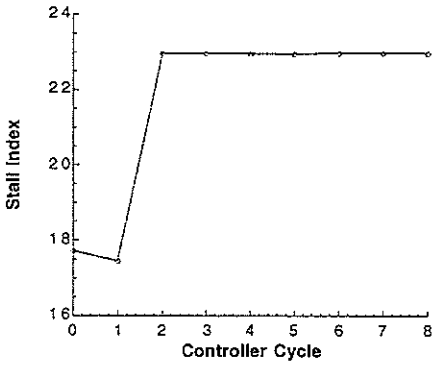

Fig. 7. Response of stall index to controller with 2P and 4P input ($\mu = 0.236$, $C_T/\sigma = 0.13$).

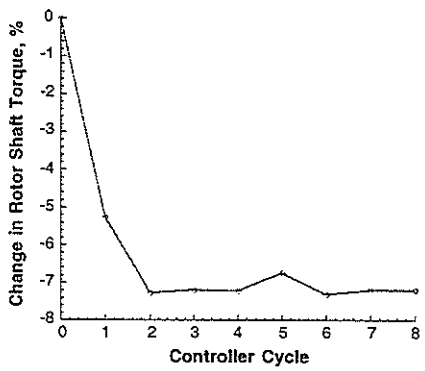

Fig. 8. Reduction in rotor shaft torque with 2P controller ($\mu = 0.236$, $C_T/\sigma = 0.13$).